

# Generic surface modification strategy for sensing applications based on Au/SiO<sub>2</sub> nanostructures

Rodolphe Marie, Andreas B. Dahlin, Jonas O. Tegenfeldt, and Fredrik Höök<sup>a)</sup>  
Lund University, Division of Solid State Physics, P.O. Box 118, SE-221 00 Lund, Sweden

(Received 26 January 2007; accepted 28 February 2007; published 29 March 2007)

A generic protocol for the creation of material-mediated self-assembled patterns of streptavidin, defined solely by patterns of gold and SiO<sub>2</sub>, is presented. Protein-adsorption resistance of selected regions was obtained by material-specific adsorption of thiol-modified poly(ethylene)glycol (thiol-PEG) on gold followed by adsorption of poly-L-lysine (PLL) modified PEG (PLL-g-PEG) on SiO<sub>2</sub>. Selective streptavidin binding to either gold or SiO<sub>2</sub> (or both) was ensured by introducing biotin-modified thiolated (thiol-biotin) and/or biotin-modified PLL-g-PEG (PLL-g-PEGbiotin) compounds. The introduction of biotin did not influence the protein-adsorption resistance. On the macroscopic scale, the protein-adsorption-resistant properties and the streptavidin-binding capacity were optimized using quartz crystal microbalance with dissipation monitoring. The reproduction of micrometer-scale gold patterns on SiO<sub>2</sub> into patterns of streptavidin was verified using fluorescence microscopy, while the compatibility of the material-specific surface-modification strategy with nanoscale features was accomplished by modifying a localized surface plasmon resonance (LSPR) active template, defined by randomly distributed nanoapertures in a thin gold film on SiO<sub>2</sub>. The demonstrated compatibility of the latter substrate with LSPR-based label-free sensing of biorecognition reactions, combined with the fact that all compounds utilized are commercially available, makes the surface-modification protocol attractive as a generic surface modification solution for a broad range of biorecognition-based assays. © 2007 American Vacuum Society. [DOI: 10.1116/1.2717926]

## I. INTRODUCTION

Significant work within life science is currently devoted to surface patterning of biomolecules as templates for ligand binding in, for example, DNA-hybridization and immuno assays. In principle every ligand/receptor pair can be transferred into a surface-based assay, but in practice the immobilization of ligand and/or receptor molecules is challenged by the fact that most ligand-receptor reactions are sensitive to the orientation and the conformation of the immobilized component. Furthermore, efficient strategies are required for immobilization of different entities to predefined spots in high-density arrays. Generally, (bio)chemically active areas are generated by chemically patterning the surface used for site-selective binding of predefined ligands, whereas remaining areas are made inert to nonspecific biomolecular adsorption. Pin spotting and ink-jet printing were developed for the production of DNA microarrays and are today in widespread use.<sup>1,2</sup> More recently, UV-masking techniques were introduced for *in situ* solid-phase synthesis of oligonucleotides.<sup>3</sup> Various contact and noncontact printing techniques, including microcontact printing using polydimethoxy-silane (PDMS) stamps, have been used for the creation of DNA and protein patterns on flat<sup>4,5</sup> and, more recently, microstructured substrates.<sup>6</sup> In the latter case, protein microarrays were printed on microchannels before sealing of a microfluidic device, thus enabling microfluidics to be combined with array-based readout. However, since printing techniques im-

ply drying of the biomolecule-containing “ink,” they are inappropriate for patterning of probe molecules that are sensitive to denaturation upon drying. For example, less robust proteins may unfold on the surface, which might severely influence their ability to bind ligands. Moreover, printing techniques are not applicable on molecular assemblies that cannot be dried, such as supported lipid assemblies<sup>7</sup> or cells. Finally, when working with low-abundance ligands, it is critical that all binding reactions are localized to the site of detection,<sup>8</sup> which, in turn, put strong constraints on the repellent properties of the areas surrounding the active sites.

In this work, we present a generic surface-modification protocol enabling self-assembled patterns of streptavidin to be generated solely defined by nanoscale patterns of gold on SiO<sub>2</sub>. Different strategies relying on self-assembly of receptor molecules on chemically patterned substrates were previously demonstrated.<sup>9–11</sup> The merit of self-assembly is primarily that drying of the receptor molecules can be circumvented and that it is generally compatible with parallel array formation. Lee *et al.* reported a self-assembly strategy to immobilize DNA on a gold substrate that was premodified with thiolated coupling agents which were subsequently activated by UV masking, allowing efficient coupling of thiolated DNA.<sup>9</sup> Surrounding inert areas were generated by coupling of poly(ethylene glycol) (PEG) chains. This approach provides arrays of DNA separated by protein-adsorption resistant areas, thus enabling the enzymatic digestion of DNA to be probed on array format. Stamou *et al.* used microcontact printing for patterning of bovine serum albumin (BSA) and biotinylated BSA on SiO<sub>2</sub>, prior to self-

<sup>a)</sup>Electronic mail: fredrik.hook@ftf.lth.se

assembly of lipid vesicles.<sup>10</sup> Microcontact printing has also been widely used for defining cell-adhesive and inert patterns (see Ref. 12 and references therein). In yet another approach, Falconnet *et al.* combined imprinting with self-assembly by first defining a pattern in a polymer using nanoimprint lithography.<sup>11</sup> This was followed by self-assembly of a biotinylated copolymer. When later the polymer resist was dissolved in acetone, remaining areas were made inert by self-assembly of poly-L-lysine (PLL)-*g*-PEG, thus creating a biotinylated pattern in a stepwise and highly parallel process. These techniques all enable chemical patterns to be created on chemically homogeneous substrates (thiols on gold<sup>9</sup> and physisorption<sup>10,11</sup>). However, neither of these methods is easily extended to the creation of chemical patterns on sub-100 or sub-10 nm length scales. Hence, to reach the vision of chemical patterns of down to single receptor molecules, there is a need of alternative surface modification strategies.

To reach these length scales, self-assembly on templates defined by patterns of different materials is an attractive approach. In this case, self-assembly is solely directed by the surface properties of alternated materials, which implies that the functionalization of different regions can be made stepwise and independently. Metal patterns on SiO<sub>2</sub> are easily mass produced using lift-off techniques combined with conventional UV lithography and various nanofabrication procedures such as E-beam lithography, nanoimprint lithography, colloidal lithography, and focused ion beam lithography (see Ref. 13 and references therein). Of particular interest in sensor applications are gold patterns on SiO<sub>2</sub>, primarily because thiolated DNA and proteins can be self-assembled in a single-step procedure. Moreover, SiO<sub>2</sub> can be modified independently of gold using either physisorption or silane chemistry, making this material attractive in defining the “passive” region of the sensor.<sup>14–18</sup> Arnold *et al.* recently demonstrated nanometer-scale surface patterns of colloidal gold particles on SiO<sub>2</sub> using a combined silane/thiol strategy, enabling the influence of attachment geometry on cell behavior to be studied in detail.<sup>14</sup> We recently extended the material specific biotin-BSA adsorption on gold over SiO<sub>2</sub> for site-selective binding of vesicles from micro-scale<sup>15</sup> to nanoscale dimensions.<sup>16</sup> However, in terms of reducing nonspecific adsorption of vesicles, PEG is superior over BSA, as demonstrated on both the microscale<sup>17</sup> and the nanoscale.<sup>18</sup> In the latter work, nanoscale pillars of TiO<sub>2</sub> were defined on SiO<sub>2</sub> using colloidal lithography. The TiO<sub>2</sub> pattern was transformed into a streptavidin pattern using stepwise modification of TiO<sub>2</sub> and SiO<sub>2</sub>, by first making TiO<sub>2</sub> hydrophobic using phosphate dodecyl and then SiO<sub>2</sub> inert using adsorption of PLL-*g*-PEG. Finally, streptavidin was physisorbed on the hydrophobic TiO<sub>2</sub> pillars.

In this work we demonstrate how PLL-*g*-PEG in combination with thiolated PEG can be used to create nanoscale patterns of SiO<sub>2</sub> and/or gold inert, while both materials can be independently activated with functional groups by addition of biotinylated PLL-*g*-PEG and/or biotinylated thiol-PEG,<sup>19</sup> as schematically shown in Fig. 1. In this way

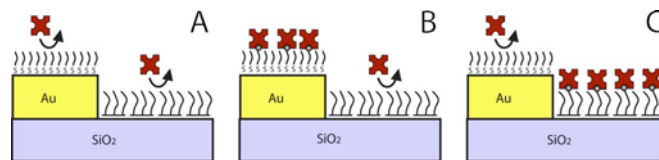


FIG. 1. Schematic description of the surface modification. (A) Gold was coated using thiol-modified PEG carrying a terminal hydroxyl group. Silicon dioxide was coated with PLL-*g*-PEG, a copolymer adsorbing electrostatically through its polylysine backbone, thus exposing its PEG chains toward the suspension. Both surfaces are shown to be inert to streptavidin and serum finding. When using the biotinylated form of either of the PEG coatings, streptavidin could be selectively bound to either gold (B) or SiO<sub>2</sub> (C).

either gold or SiO<sub>2</sub> can be independently modified with streptavidin, thus providing a generic template for the creation of supramolecular architectures engaging, for example, biotinylated nucleic acids, antibodies, lipid vesicles, or a combination thereof.

Efficient and selective binding of streptavidin to each of the two materials is demonstrated on the macroscopic scale using quartz crystal microbalance with dissipation (QCM-D) monitoring, while selective immobilization of streptavidin on gold and SiO<sub>2</sub> is demonstrated on the micron scale using fluorescence microscopy. To verify the success of the surface modification strategy on the nanometer length scale, we made use of the color changes associated with changes in interfacial refractive index of localized surface plasmon resonance (LSPR) active cylindrical nanometric apertures (Ø110 nm) in thin (55 nm) gold films on SiO<sub>2</sub>.<sup>16</sup> By monitoring the temporal variations of the extinction peak position of the LSPR active substrate, it is demonstrated that SiO<sub>2</sub> can be selectively modified using PLL-*g*-PEG after completed modification of gold using thiol-PEG. By introducing the biotinylated variants of the two compounds, selective coupling of streptavidin to either gold, SiO<sub>2</sub>, or both is proven feasible. The LSPR response obtained upon selective binding of streptavidin on the different regions is compared with the streptavidin coverage on homogeneous SiO<sub>2</sub> and gold substrates, and discussed on the basis of the expected field distribution within LSPR active nanoscale cylindrical apertures.

## II. RESULTS AND DISCUSSION

### A. QCM-D measurements

Prior to QCM-D measurements, gold-coated crystals were modified by overnight incubation in a 1 mM ethanol thiol-PEG suspension. The repellent properties of thiol-PEG-coated gold was investigated by addition of a human serum suspension (5% in buffer), yielding a frequency shift of  $-1.7 \pm 0.9$  Hz, which corresponds to 2% of full protein coverage ( $\sim -80$  Hz). Nonspecific binding of streptavidin (160 nM) was below the detection limit ( $-0.2$  Hz) (Table I). Specific binding of streptavidin on gold was obtained using thiol-PEGbiotin. However, a pure thiol-PEGbiotin layer did not only yield a high binding of streptavidin ( $-16.6$  Hz) but also significant binding of PLL-*g*-PEG ( $-16.6$  Hz). Since the aim of the patterning strategy was to independently modify

TABLE I. Changes in frequency (and relative coverage in percentage) upon binding of PLL-*g*-PEG and streptavidin on differently coated gold and SiO<sub>2</sub> modified crystals. Prior to exposure of either PLL-*g*-PEG or streptavidin gold was coated with either thiol-PEG or thiol-PEG/PEGbiotin and SiO<sub>2</sub> was coated with either PLL-*g*-PEG or PLL-*g*-PEG/PEGbiotin. When measured, the changes of frequency for the coating itself are shown. N.D. means not determined. The errors reflect the typical reproducibility over replicate experiments.

Substrate	Coating	Frequency shift (-Hz) (percentage of full coverage)		
		Coating itself	PLL- <i>g</i> -PEG	Streptavidin
Gold	Thiol-PEG	N.D.	1.5 (5%)	<0.2 (<0.7%)
Gold	Thiol-PEGbiotin	N.D.	16.6 (59%)	16.6 (78%)
Gold	Thiol-PEG/PEGbiotin	N.D.	1.7 (6%)	21.2 (100%)
SiO <sub>2</sub>	PLL- <i>g</i> -PEG	28.2 (100%)	<0.2 (<0.7%)	<0.2 (<0.7%)
SiO <sub>2</sub>	PLL- <i>g</i> -PEG/PEGbiotin	30.1 (100%)	<0.2 (<0.7%)	16.4 (100%)

gold and SiO<sub>2</sub> regions on the very same substrate, this is not satisfactory. By investigating different mixtures of thiol-PEG and thiol-PEGbiotin, it was shown that the best compromise with respect to low nonspecific binding of PLL-*g*-PEG (<5% of full coverage), but still sufficiently high streptavidin binding (-21.2 Hz), was obtained at a thiol-PEG:thiol-PEGbiotin ratio of 1:1 (Table I). The introduction of thiol-biotin at this ratio resulted in a slightly higher nonspecific serum-protein adsorption compared with that obtained using thiol-PEG alone, while introduction of PLL-*g*-PEGbiotin instead of PLL-*g*-PEG did not. Future work will concentrate on controlling the stoichiometric ratio between PEG and biotin on the surface, with respect to suppressed nonspecific protein adsorption, high streptavidin binding capacity, as well as the ability of immobilized streptavidin to subsequently capture biotinylated compounds. Note that the real nonspecific binding of PLL-*g*-PEG is, in fact, expected to be lower than that estimated from QCM-D measurements. This is so because at lower coverage, the amount of measured coupled water sensed by changes in frequency per adsorbed molecule is expected to be larger than at saturated coverage.<sup>20</sup>

In agreement with our previous studies,<sup>8</sup> *in situ* modification of SiO<sub>2</sub>-coated QCM-D sensors with PLL-*g*-PEG yielded frequency and dissipation changes of  $-28.2 \pm 4.0$  Hz and  $1.7 \pm 0.1 \times 10^{-6}$ , respectively. This suggests a 33% lower uptake of PLL-*g*-PEG on SiO<sub>2</sub> than previously obtained on Nb<sub>2</sub>O<sub>5</sub>.<sup>21</sup> However, the protein-adsorption resistant properties of PLL-*g*-PEG modified SiO<sub>2</sub> are still excellent. This was verified from the fact that binding of human serum (5%) resulted in a frequency shift of  $-0.6 \pm 0.4$  Hz, which corresponds to less than 1% of the protein uptake from serum on unmodified SiO<sub>2</sub> ( $\sim -80$  Hz). In agreement with thiol-PEG modified gold, nonspecific binding of streptavidin (160 nM) was below the detection limit. In order to provide specific binding of streptavidin on SiO<sub>2</sub>, a mixture of PLL-*g*-PEG and PLL-*g*-PEGbiotin at a ratio of 1:1 was used.<sup>19</sup> Upon exposure of SiO<sub>2</sub> modified with PLL-*g*-PEG/PEGbiotin (1:1) to streptavidin (160 nM), a saturated change in frequency of  $-16.4 \pm 1.9$  Hz was obtained. The reduction in subsequent streptavidin binding to PLL-*g*-PEG:PLL-*g*-PEGbiotin mix-

tures on SiO<sub>2</sub>, compared with that previously observed on Nb<sub>2</sub>O<sub>5</sub>, is in agreement with recent optical waveguide light-mode spectroscopy (OWLS) studies.<sup>22</sup> Furthermore, the response is 30% lower than that obtained on thiol-PEG/PEGbiotin modified gold. However, due to the relatively long PEG chains of PLL-*g*-PEG (41 units), the biotin moieties are in this case distributed within a three-dimensional matrix, while in contrast, the biotin moieties are expected to be distributed in two dimensions on thiolated gold. As a consequence, the contribution from coupled/replaced water to the frequency response is expected to differ in the two cases. This means, in turn, that quantitative comparisons should be made with great care. Nevertheless, the QCM-D response obtained for PLL-*g*-PEG/PEGbiotin on SiO<sub>2</sub> can be compared with the results obtained on Nb<sub>2</sub>O<sub>5</sub> by Städler *et al.*<sup>21</sup> who used both QCM-D and OWLS. Assuming that the ratio in mass uptake of PLL-*g*-PEG/PEGbiotin obtained on Nb<sub>2</sub>O<sub>5</sub> is conserved on SiO<sub>2</sub>, one arrives at a PLL-*g*-PEG/PEGbiotin coverage of  $\sim 145$  ng/cm<sup>2</sup> in the latter case. In the same way, by extrapolating the data on streptavidin binding to mixtures of PLL-*g*-PEG/PLL-*g*-PEGbiotin mixtures by Xu *et al.*<sup>22</sup>, this yields a streptavidin coverage of  $\sim 120$  ng/cm<sup>2</sup> in the present case. A similar streptavidin coverage of 130 ng/cm<sup>2</sup> was shown on PLL-*g*-PEG/PEGbiotin (1:1) on carboxylated thiols on gold.<sup>23</sup> This thus suggests that the coverage of streptavidin on PLL-*g*-PEG/PEGbiotin is  $\sim 60\%$  of the mass uptake previously reported using biotinylated thiols on gold (210 ng/cm<sup>2</sup>).<sup>24</sup> To support the interpretation of the LSPR data in the final section, we will therefore assume streptavidin coverages on SiO<sub>2</sub> and gold of  $\sim 120 \pm 10$  and  $\sim 210 \pm 10$  ng/cm<sup>2</sup>, respectively. Most important, however, is the fact that thiol-PEG (and thiol-PEG/PEGbiotin) modified gold is inert towards PLL-*g*-PEG (and PLL-*g*-PEGbiotin) binding, which is a prerequisite in order to independently functionalize either patterns of gold and SiO<sub>2</sub> with streptavidin.

## B. Fluorescence microscopy

To verify that gold and SiO<sub>2</sub> can be independently modified, streptavidin patterns on the micron scale were investi-

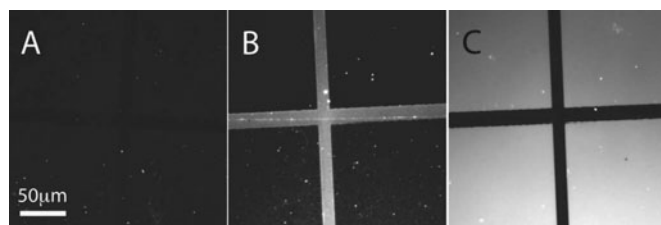


FIG. 2. Fluorescence micrographs (filters chosen for Cy3 emission) of 13  $\mu\text{m}$  wide lines of gold on a  $\text{SiO}_2$  substrate. The images were recorded after the addition of streptavidin labeled with Cy3. Gold and  $\text{SiO}_2$  were coated, respectively, with (A) thiol-PEG and PLL-*g*-PEG, (B) thiol-PEG/PEGbiotin and PLL-*g*-PEG, and (C) thiol-PEG and PLL-*g*-PEG/PEGbiotin. All images have identical contrast and brightness settings; the scale shown in (A) is the same for (B) and (C). The bright spots in the micrographs are attributed to surface defects.

gated using fluorescence microscopy. A gold pattern defined by two crossing 13  $\mu\text{m}$  wide lines on a  $\text{SiO}_2$  surface was modified using either thiol-PEG or thiol-PEG/PEGbiotin (1:1) followed by exposure to PLL-*g*-PEG or PLL-*g*-PEG/PEGbiotin. Thereafter, streptavidin, labeled with the fluorophore Cy3, was added before fluorescence micrographs were taken (Fig. 2). However, on gold essentially complete fluorescence quenching was observed, being attributed to the presence of streptavidin within 10 nm from the gold surface. Therefore, DNA was used as a spacer between streptavidin-Cy3 and a first layer of unlabeled streptavidin. This was shown to provide sufficient reduction of the quenching, thus providing a clear fluorescence contrast between gold and PLL-*g*-PEG modified  $\text{SiO}_2$  that perfectly matched the anticipated biotinylated pattern. With both materials modified with PEG chains [Fig. 2(a)], the fluorescence was comparable to the background fluorescence. In contrast, the fluorescence intensity increased dramatically on both biotinylated  $\text{SiO}_2$  [Fig. 2(c)] and gold [Fig. 2(b)], demonstrating specific binding of Cy3-labeled streptavidin determined solely by the underlying material. In particular, nonspecific binding of streptavidin to PEG-modified gold was low even after modification of  $\text{SiO}_2$  with PLL-*g*-PEG/PEGbiotin, and nonspecific binding of streptavidin was low on PLL-*g*-PEG-modified  $\text{SiO}_2$ , in which case the latter modification was made after completed modification of gold with thiol-PEG/PEGbiotin. Hence, these results demonstrate the compatibility of the surface modification strategy for micron scale patterns of gold on  $\text{SiO}_2$ .

### C. LSPR response on nanometric apertures

Measurements of the colorimetric changes of LSPR active nanometric apertures ( $\varnothing \sim 110$  nm) in a 55 nm thick gold film were used to address the compatibility of the surface modification scheme with nanoscale features composed of gold and  $\text{SiO}_2$ .<sup>25</sup> Prior to measurements, the samples were incubated in a thiol-PEG or a thiol-PEG/PEGbiotin suspension. Thereafter changes in the extinction peak position of the LSPR active substrate were monitored upon exposure to either PLL-*g*-PEG or PLL-*g*-PEG/PEGbiotin. Figure 3 displays the temporal variations in the peak position upon ad-

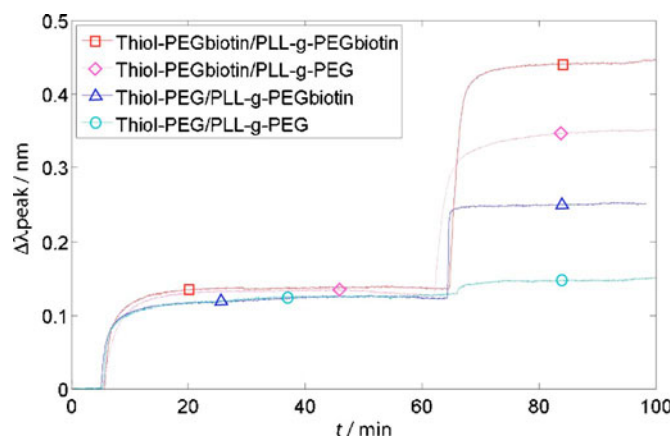


FIG. 3. LSPR data: changes in (centroid) peak position,  $\Delta\lambda_{\text{peak}}$ , vs time upon adsorption of PLL-*g*-PEG (PLL-*g*-PEG/PEGbiotin) (10  $\mu\text{g}/\text{ml}$ ) and the subsequent binding of streptavidin (10  $\mu\text{g}/\text{ml}$ ) for four different combinations of coatings of gold and  $\text{SiO}_2$  inside the apertures. Before addition of streptavidin the volume exposed to the surface was rinsed fence with 3 ml buffer. The peak position exhibits a typical noise of  $3 \times 10^{-3}$  nm (Ref. 25).

dition of PLL-*g*-PEG or PLL-*g*-PEG/PEGbiotin ( $t=5$  min) for the four possible combinations: (i) both gold and  $\text{SiO}_2$  modified with biotin, either (ii) gold or (iii)  $\text{SiO}_2$  modified with biotin, or (iv) both materials modified with PEG.

PLL-*g*-PEG adsorption yields a peak position shift of 0.12 nm when gold is modified with PEG, and a 6% higher peak position shift in the two cases when gold was modified with thiol-PEG/PEGbiotin (squares and diamonds in Fig. 3). This is consistent with the slightly larger adsorption of PLL-*g*-PEG on the biotinylated thiol layer than on a plain thiol-PEG layer observed using QCM-D (Table I). Upon addition of streptavidin ( $t \sim 65$  min) binding on both  $\text{SiO}_2$  and gold yields a peak position change of 0.31 nm, which thus constitutes the maximum obtainable response of the sensor template to streptavidin binding. For the sample coated with thiol-PEG prior to the addition of PLL-*g*-PEG, nonspecific streptavidin binding corresponds to 6% (0.02 nm) of the total response, thus demonstrating that the coatings of gold and  $\text{SiO}_2$  with PEG provide high protein-repellent properties also on features with nanoscale topography. This is consistent with the fact that the dimensions of both PLL-*g*-PEG and thiol-PEG molecules are significantly smaller than the topographic features of the substrate. Nevertheless, the nonspecific binding is somewhat higher than expected based on the QCM-D results on planar surfaces. Tentatively, the slight increase in nonspecific binding is attributed to the border between  $\text{SiO}_2$ , gold, and the adhesion chromium layer. In this region, the two PEG coatings meet in a region likely to contain a pronounced defect density, which means that the compound cannot overlap as efficiently as on the homogeneous regions. Moreover, this border is located at the lower edge of the gold film [Fig. 4(a)], where the plasmonic field is expected to be highest (see also below).<sup>26–28</sup> This means, in turn, that binding in this region is expected to contribute more to the total response than do binding events that occur elsewhere on the substrate (see further below). Nevertheless, since the peak position shifts upon binding of streptavidin on

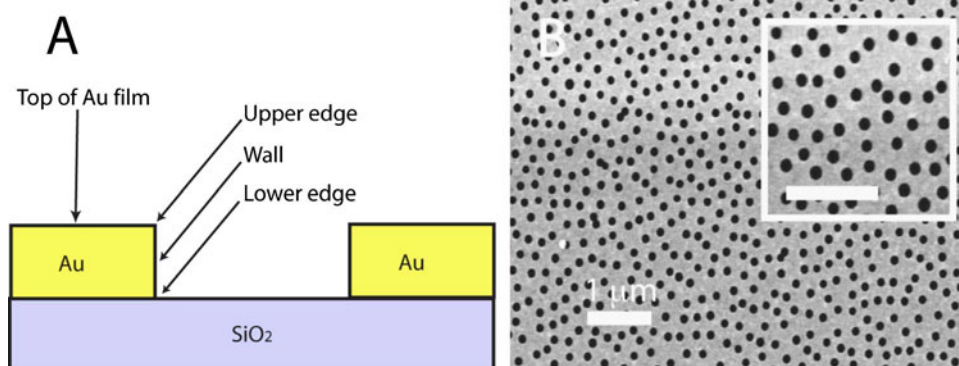


FIG. 4. (A) Schematic side view of the gold film with a cylindrical aperture displaying the top of the Au film *outside* the apertures, the cylindrical wall *inside* the apertures and the lower and upper edges of the Au film at the aperture. (B) Scanning electron microscopy image of the randomly distributed circular apertures in a gold film on SiO<sub>2</sub> used for localized surface plasmon resonance (LSPR) measurements. Apertures are 110 nm in diameter and 55 nm in depth. The inset is a close-up on a  $2 \times 2 \mu\text{m}^2$  area. Scale bars are 1  $\mu\text{m}$ .

either gold (diamonds) or SiO<sub>2</sub> (triangles) perfectly add up to the maximum peak shift, the defects in the PEG coating do not significantly influence the material-specific and thus site-selective guidance of streptavidin binding. Furthermore, the fact that the LSPR responses upon selective binding on SiO<sub>2</sub> or gold add up to the response upon binding on both gold and SiO<sub>2</sub> demonstrates that the response upon binding on gold is uncoupled from the response upon binding on SiO<sub>2</sub>; that is, a change in interfacial refractive index in one region (gold or SiO<sub>2</sub>) does not affect the refractive index sensitivity of the other (SiO<sub>2</sub> or gold). This finding, combined with the estimate of the mass uptake of streptavidin on gold and SiO<sub>2</sub> (see above), is in the final section used to qualitatively estimate the plasmonic field distribution associated with the randomly distributed cylindrical apertures.

#### D. Quantification of the LSPR response

The redshift upon binding of streptavidin on SiO<sub>2</sub> (triangles in Fig. 3) in the bottom of 110 nm wide and 55 nm deep cylindrical apertures corresponds to 39% of the maximum response of the sensor template (circles in Fig. 3). Considering that SiO<sub>2</sub> represents no more than  $\sim 10\%$  of the total area exposed [including the cylindrical wall of the apertures as depicted in Fig. 4(a)] to streptavidin, this confirms a high localization of the plasmonic field to the voids of the holes.<sup>16,25</sup> To use this observation to estimate the field distribution within the aperture, it is useful to first assume that the plasmonic field is homogeneously distributed within the void of the holes and that binding on the gold substrate outside the holes does not contribute to a change in the peak position. If this is the case, the ratio between the response upon binding on SiO<sub>2</sub> and gold is expected to reflect the ratio between the area of the cylindrical wall (gold) and the area of the bottom (SiO<sub>2</sub>) of the holes [Fig. 4(a)]. With the current dimensions, the expected area ratio between gold and SiO<sub>2</sub> within the aperture is  $\sim 2$ , which is in fairly good agreement with the experimentally observed ratio of 1.75 (0.21 nm/0.12 nm). However, taking into account the fact that the coverage of

streptavidin on gold ( $\sim 210 \text{ ng/cm}^2$ ) is 1.6 times higher than on SiO<sub>2</sub> ( $\sim 130 \text{ ng/cm}^2$ ), it is evident that the sensitivity is highly localized to the *bottom* rather than the *walls* of the holes. Furthermore, recent theoretical estimations of the plasmonic field associated with cubic<sup>26</sup> and triangular<sup>27,28</sup> noble metal nanoparticles suggest a field enhancement at the edges of the structures. Translating these results to cylindrical apertures, the field is expected to be enhanced at the top and the bottom of the voids. This means, in turn, that the field is expected to extend also on the gold film outside the holes, thus violating our initial assumption regarding a homogeneous field within the void of the holes. As a consequence, the gold area that contributes to the signal is expected to be even larger than that of the cylindrical walls alone, pointing towards an even higher localization of the effective sensitivity to the bottom of the apertures. Indeed, the large response (per unit area) upon binding on the bottom of the holes reflects, most likely, the fact that this region is located within the evanescent electric field associated with the lower edge of the aperture. A similar field enhancement is expected also at the top of the apertures. However, since streptavidin binding on gold yields a relatively low response, it is concluded that the sensitivity of changes in interfacial refractive index upon binding on the gold film outside the apertures decays rapidly with distance from the upper edge of the apertures.

### III. CONCLUSIONS

We demonstrate in this work that a combination of thiol-PEG and PLL-*g*-PEG chemistry is suitable for modifications of patterned substrates composed of gold and SiO<sub>2</sub>. The generic nature of the strategy makes it likely to be suitable for a large range of applications, ranging from ordered arrays of nanoscale apertures for surface-enhanced Raman scattering and enhanced fluorescence applications as recently reported by Brolo *et al.*<sup>29,30</sup> to patterns of nanostructures defined by, for example, electron beam lithography or focused ion beam lithography, which enable the creation of predefined patterns on various length scales. Furthermore, by combining optical spectrophotometry of LSPR active substrates with this type

of material-specific surface modifications and, for example, layer-by-layer formation of molecular multilayer<sup>31</sup> detailed insights into the local field distribution can be mapped out. While generic theories capable of representing the LSPR behavior of complex structures are still under development, ways of experimentally verifying such theoretical predictions are important. Furthermore, with a biotinylated template, avidin and its analogues are ideally suited for capturing of nanosized objects such as, metal nanoparticles, quantum dots, and/or lipid vesicles to predefined spots, where, for instance, sequence specific and site-selective coupling using DNA hybridization<sup>21,31</sup> may even open up for the creation of dense arrays, using, e.g., dip-pen nanolithography methods, enabling each spot to carry a unique specificity. Alternatively, randomized size-exclusive positioning followed by postidentification of binding reactions is another interesting approach.

Hence, the concept may eventually be proven valuable in a vast amount of bioanalytical assays relying on DNA hybridization, enzymatic activity, immuno-complex formation or, using supported lipid membrane assemblies, cell-membrane-mediated biorecognition reactions. Once transferred to the level of single molecules and in combination with nanofluidics,<sup>32</sup> utterly sensitive detection methods<sup>33</sup> and barcoding assays<sup>34,35</sup> multiplexed single molecule diagnostics might eventually be realized.

## IV. MATERIALS AND METHODS

### A. QCM-D, fluorescence microscopy, and LSPR

The QCM-D instrument and all measurements were from Q-Sense AB (Q-sense, D300). The noise in combined frequency and energy dissipation QCM-D measurements was  $\sim 0.2$  Hz and  $\sim 0.05 \times 10^{-6}$ , respectively. Fluorescence micrographs of immobilized streptavidin-Cy3 were imaged using a Nikon Eclipse TE2000-U microscope (Nikon Co., Japan) equipped with an electron multiplying charge-coupled device (EMCCD) camera (model iXon DV887-BI, Andor Technology, UK) cooled to  $-50$  °C and used in combination with a Nikon TRITC filter set. LSPR measurements were made on a homebuilt instrument.<sup>25</sup> The substrate was mounted on a homebuilt flow cell, allowing the liquid in contact with the surface to be rapidly ( $< 1$  s) exchanged. Temporal variations in the peak position,  $\Delta\lambda_{\text{peak}}$ , were monitored by tracking the center-of-mass position of the extinction peak as described elsewhere.<sup>25</sup> The flow cell was incubated overnight in 1% sodium dodecyl sulfate (SDS), rinsed with water, cleaned for 20 min in UV/ozone, and coated with PLL-*g*-PEG before each experiment.

### B. Substrates

All QCM sensor crystals (AT-cut quartz crystals,  $F_0 = 5$  MHz, with either gold or SiO<sub>2</sub> coating) were from Q-sense AB, Sweden. Gold-coated crystals were cleaned for 1 h in UV/ozone (FHR UVOH150) prior to any modification. Silicon dioxide coated crystals were incubated overnight in 1% aqueous SDS (Sigma-Aldrich, Germany) sus-

pension and cleaned for 20 min in UV/ozone before being mounted in the QCM-D measurement cell, allowing online monitoring of surface modifications. Substrates (micron sized patterns of gold on SiO<sub>2</sub>) for fluorescence measurements were fabricated using conventional UV lithography, by depositing 20 nm of gold on a 10 nm adhesion layer of chromium through a double layer lift-off resist mask (LOR 3A, Microchem and S1813, Shipley) on 40 nm SiO<sub>2</sub> thermally grown on a silicon wafer. The samples were cleaned before surface modifications by sonication ( $\sim 1$  min) in 1% aqueous SDS suspension followed by 1 h UV/ozone (FHR UVOH150). The fluorescence of the streptavidin-Cy3 bound to the samples was imaged using a Nikon Eclipse TE2000-U microscope (Nikon Co., Japan) equipped with an EMCCD camera (model iXon DV887-BI, Andor Technology, UK) cooled to  $-50$  °C used in combination with a Nikon TRITC filter set. All images in Fig. 2 have identical contrast and brightness settings. The LSPR active gold film with nanometric apertures was prepared by colloidal lithography, as described elsewhere.<sup>16</sup> Glass substrates were 0.7 mm thick borosilicate SiO<sub>2</sub> (Schröder Glass, Germany) cleaned in piranha suspension (H<sub>2</sub>SO<sub>4</sub>+30% H<sub>2</sub>O<sub>2</sub>, 3:1 volume) for 10 min prior to the deposition of 110 nm polystyrene sulfate colloids (IDC, Oregon, USA). Chromium (2 nm, Cerac, USA) was used as an adhesion layer before depositing gold (53 nm, Dahlgren Ädelmetall, Sweden), thus producing circular apertures with rectangular profiles in the gold film. Metals were deposited by thermal evaporation at  $5 \times 10^{-5}$  Pa (AVAC system, Sweden) using a reference quartz crystal microbalance to determine the film thickness. After particle lift-off using tape, the nanostructures were characterized with field emission scanning electron microscopy (JEOL JSM6400F) [Fig. 4(b)]. The sample was reused and cleaned before each measurement by sonication ( $\sim 1$  min) in 1% aqueous SDS suspension followed by 1 h UV/ozone (FHR UVOH150), proven sufficient to clean the samples.<sup>16</sup>

### C. Surface modifications

Gold was modified using thiols which were dissolved in ethanol (99.7%, Solveco Chemicals AB, Sweden) at a concentration of 1 mM. The thiolated PEG was a linear polyethylene glycol chain with six PEG units, a terminal hydroxyl group, and an undecyl linker with a thiol group (Prochimia, Poland). The biotinylated thiol-PEG (thiol-PEGbiotin) was purchased as a disulfide dimer (Polypure, Norway), with each monomer being a linear PEG chain with eight units and modified with a biotin moiety in the end. The modification of gold surfaces was made by incubation overnight in the ethanolic suspension followed by sonication in ethanol for 2 min. The surface was rinsed in ethanol and water and dried in nitrogen prior to use. SiO<sub>2</sub> was modified with PLL-*g*-PEG and PLL-*g*-PEGbiotin (Surface Solutions, Switzerland) at a concentration of 10  $\mu\text{g}/\text{ml}$  dissolved in 4-(2-hydroxyethyl)-1-piperazineethanesulfonic acid (HEPES) buffer (10 mM HEPES, 100 mM NaCl, pH 7.4). The samples patterned with gold and silicon dioxide were first incubated in either thiol-PEG or thiol-PEG/PEGbiotin suspension (1 mM

in EtOH) overnight, sonicated (Branson 1510) in pure ethanol for 2 min, rinsed in ethanol and water, and dried under nitrogen. While the subsequent steps of the LSPR active substrates were analyzed *in situ*, the patterned substrates used for fluorescence microscopy were modified by incubation in PLL-*g*-PEG or a 1:1 mixture of PLL-*g*-PEG/PEGbiotin for 50 min, after which the surface was rinsed in buffer. LSPR active samples were coated with streptavidin until saturation of the signal, whereas patterned samples for fluorescence microscopy were incubated in a suspension containing streptavidin:DNAa complex for 40 min. After rinsing in buffer, the surface was incubated for another 40 min in a suspension of streptavidin-Cy3:DNAb complex and rinsed in buffer. Streptavidin and streptavidin-Cy3 (Sigma, Germany) were mixed with DNAa and DNAb, respectively (Medprobe, Norway), at a ratio of two DNA strands per streptavidin at a final concentration of 10  $\mu\text{g}/\text{ml}$  of streptavidin and allowed to react for 15 min before being introduced to the surface.<sup>21</sup> DNAa is a 15 $\nu$ mer single-stranded sequence (5-biotin-ACG TCA GTC TCA CCC-3) complementary to the 3 $\nu$ end of DNAb, a 50 $\nu$ mer single-stranded sequence (5-biotin-AGT TAC AGA GGT AGT AGT GGC TGA GTG AAT ATT GT G GGT GAG ACT GAC GT-3). Both sequences were biotinylated at their 5 $\nu$ end.

## ACKNOWLEDGMENTS

The project is supported through funding from the EU through the integrated projects NaPa (Contract No. NMPO4-CT-2003-500120-2) and Nanocues (Contract No. NMP4-CT-2003-505868), the Swedish Research Council (Grant No. 2002-5972), and through an INGVAR grant from the Swedish Strategic Research Foundation.

<sup>1</sup>M. Dufva, *Biomol. Eng.* **22**, 173 (2005).

<sup>2</sup>V. G. Cheung, M. Morley, F. Aguilar, A. Massimi, R. Kucherlapati, and G. Childs, *Nat. Genet.* **21**, 15 (1999).

<sup>3</sup>S. P. A. Fodor, J. L. Read, M. C. Pirrung, L. Stryer, A. T. Lu, and D. Solas, *Science* **251**, 767 (1991).

<sup>4</sup>A. Bernard, J. P. Renault, B. Michel, H. R. Bosshard, and E. Delamarche, *Adv. Mater. (Weinheim, Ger.)* **12**, 1067 (2000).

<sup>5</sup>J. P. Renault *et al.*, *J. Phys. Chem. B* **107**, 703 (2003).

<sup>6</sup>J. Foley, H. Schmid, R. Stutz, and E. Delamarche, *Langmuir* **21**, 11296

(2005).

<sup>7</sup>P. S. Cremer and S. G. Boxer, *J. Phys. Chem. B* **103**, 2554 (1999).

<sup>8</sup>R. Marie, J. P. Beech, J. Vörös, J. O. Tegenfeldt, and F. Höök, *Langmuir* **22**, 10103 (2006).

<sup>9</sup>H. J. Lee, Y. Li, A. W. Wark, and R. M. Corn, *Anal. Chem.* **77**, 5096 (2005).

<sup>10</sup>D. Stamou, C. Duschl, E. Delamarche, and H. Vogel, *Angew. Chem., Int. Ed.* **42**, 5580 (2003).

<sup>11</sup>D. Falconnet, D. Pasqui, S. Park, R. Eckert, H. Schiff, J. Gobrecht, R. Barbucci, and M. Textor, *Nano Lett.* **4**, 1909 (2004).

<sup>12</sup>D. Falconnet, G. Csucs, H. M. Grandin, and M. Textor, *Biomaterials* **27**, 3044 (2006).

<sup>13</sup>Y. Chen and A. Pépin, *Electrophoresis* **22**, 187 (2001).

<sup>14</sup>M. Arnold, E. Ada Cavalcanti-Adam, R. Glass, J. Blümmel, W. Eck, M. Kantlehner, H. Kessler, and J. P. Spatz, *ChemPhysChem* **5**, 383 (2004).

<sup>15</sup>S. Svedhem, I. Pfeiffer, C. Larsson, C. Wingren, C. Borrebaeck, and F. Hook, *ChemBioChem* **4**, 339 (2003).

<sup>16</sup>A. Dahlin, M. Zach, T. Rindzevicius, M. Kall, D. S. Sutherland, and F. Hook, *J. Am. Chem. Soc.* **127**, 5043 (2005).

<sup>17</sup>C. Hoffmann and G. E. M. Tovar, *J. Colloid Interface Sci.* **295**, 427 (2006).

<sup>18</sup>R. Michel, I. Reviakine, D. Sutherland, C. Fokas, G. Csucs, G. Danuser, N. D. Spencer, and M. Textor, *Langmuir* **18**, 8580 (2002).

<sup>19</sup>N. P. Huang, J. Vörös, S. M. De Paul, M. Textor, and N. D. Spencer, *Langmuir* **18**, 220 (2002).

<sup>20</sup>F. Höök, C. Larsson, and C. Fant, *Encyclopedia of Surface and Colloid Science* (Marcel Dekker, New York, 2001), pp. 774–791.

<sup>21</sup>B. Städler, D. Falconnet, I. Pfeiffer, F. Höök, and J. Vörös, *Langmuir* **20**, 11348 (2004).

<sup>22</sup>F. Xu, G. Zhen, M. Textor, and W. Knoll, *BioInterphases* **1**, 73 (2006).

<sup>23</sup>Y. Zhou, H. Xu, A. B. Dahlin, J. Gustafson, C. A. K. Borrebaeck, C. Wingren, B. Lieberg, and F. Höök, *BioInterphases* (accepted).

<sup>24</sup>G. Stengel and W. Knoll, *Nucleic Acids Res.* **33**, 69 (2005).

<sup>25</sup>A. B. Dahlin, J. O. Tegenfeldt, and F. Höök, *Anal. Chem.* **78**, 4416 (2006).

<sup>26</sup>L. J. Sherry, S.-H. Chang, G. C. Schatz, and R. P. Van Duyne, *Nano Lett.* **5**, 2034 (2005).

<sup>27</sup>A. J. Haes, S. Zou, G. C. Schatz, and R. P. Van Duyne, *J. Phys. Chem. B* **108**, 109 (2004).

<sup>28</sup>A. J. Haes, S. Zou, G. C. Schatz, and R. P. Van Duyne, *J. Phys. Chem. B* **108**, 6961 (2004).

<sup>29</sup>A. G. Brolo, R. Gordon, B. Leathem, and K. L. Kavanagh, *Langmuir* **20**, 4813 (2004).

<sup>30</sup>A. G. Brolo, S. C. Kwok, M. G. Moffitt, R. Gordon, J. Riordon, and K. L. Kavanagh, *J. Am. Chem. Soc.* **127**, 14936 (2005).

<sup>31</sup>W. Knoll *et al.*, *Colloids Surf., A* **161**, 115 (2000).

<sup>32</sup>J. T. Mannion and H. G. Craighead, *Biopolymers* **85**, 131 (2007).

<sup>33</sup>L. C. Brousseau, *J. Am. Chem. Soc.* **128**, 11346 (2006).

<sup>34</sup>Y. Wei, C. Cao, R. Jin, and C. A. Mirkin, *Science* **297**, 1536 (2002).

<sup>35</sup>R. Jin, Y. C. Cao, C. S. Thaxton, and C. A. Mirkin, *Small* **2**, 375 (2006).